JGR Oceans

RESEARCH ARTICLE
10.1029/2019JC015361

Large-Scale Fresh and Salt Water Exchanges in the Indian Ocean

Corinne B. Trott[1], Bulusu Subrahmanyam[2], V. S. N. Murty[3], and Jay F. Shriver[4]

[1]School of Ocean Science and Engineering, University of Southern Mississippi, Stennis Space Center, MS, USA, [2]School of the Earth, Ocean, and Environment, University of South Carolina, Columbia, SC, USA, [3]Council of Scientific and Industrial Research (CSIR)-National Institute of Oceanography Regional Centre, Visakhapatnam, India, [4]Open Ocean Processes and Predictions Branch, Code 7323, U.S. Naval Research Laboratory, Stennis Space Center, MS, USA

Key Points:
- A decadal analysis of salt and volume transports was conducted in the Indian Ocean
- Decadal trends E-P reveal increasingly P-dominant (E-dominant) conditions over the BoB (AS)
- We find the Indian Ocean is a salt exporter to the Southern Ocean

Supporting Information:
- Supporting Information S1
- Figure S1

Correspondence to:
C. B. Trott,
corinne.trott.ctr@nrlssc.navy.mil

Citation:
Trott, C. B., Subrahmanyam, B., Murty, V. S. N., & Shriver, J. F. (2019). Large-scale fresh and salt water exchanges in the Indian Ocean. *Journal of Geophysical Research: Oceans*, *124*. https://doi.org/10.1029/2019JC015361

Received 9 JUN 2019
Accepted 29 JUL 2019
Accepted article online 02 AUG 2019

Abstract Upper-ocean dynamics in the Northern Indian Ocean (NIO) depend on changes in the magnitude and location of the high salinity waters of the Arabian Sea and low salinity waters of the Bay of Bengal. The large sea surface salinity (SSS) differences between these two basins are related to the surface freshwater flux (evaporation minus precipitation), which is positive (negative) in the Arabian Sea (Bay of Bengal). To quantify large-scale salinity changes on decadal time scale over the whole water column and to study trends in salinity and volume transport, we have analyzed Simple Ocean Data Assimilation (SODA) reanalysis product, HYbrid Coordinate Ocean Model (HYCOM) simulations, European Centre for Medium-Range Weather Forecasting's ERA-Interim reanalysis product, and riverine streamflow data from the National Centers for Atmospheric Research's Global River Flow and Continental Discharge Dataset for the NIO. We find increased freshening conditions in the Bay of Bengal and salinification conditions in the Arabian Sea that would support a stronger zonal SSS difference in the NIO but that it is partially compensated by positive (negative) salt transports into the Bay of Bengal (BoB) (Arabian Sea). Empirical orthogonal function analysis of SODA SSS indicates that the main factors of SSS variability are Indian Ocean Dipole and El Niño-Southern Oscillation and seasonal currents. The trends in the volume transport reveal decadal changes in zonal equatorial currents in HYCOM and Somali Current in SODA.

Plain Language Summary Salinity in the Indian Ocean responds strongly to a variety of processes, including advection by monsoonal and equatorial currents, surface freshwater flux from an imbalance between evaporation and precipitation rates, and discharge from local river systems. The Arabian Sea in the northwestern Indian Ocean is an evaporation-dominant region with low riverine discharge, and the Bay of Bengal in the northeastern Indian Ocean experiences extremely high seasonal precipitation and is the outflow region for major river systems such as the Ganges-Brahmaputra Delta, resulting in significantly lower salinity. To better understand large-scale changes in salinity, this study analyzes these processes over a decadal period using the HYbrid Coordinate Ocean Model and Simple Ocean Data Assimilation reanalysis product. We find interesting results, such as an increasing imbalance in surface freshwater flux between the basins, compensated by increased salinity advection. Additionally, events such as the Indian Ocean Dipole and El Niño-Southern Oscillation were found to play a role in the year-to-year salinity distributions, which we confirmed with an empirical orthogonal function analysis. Conditions in the southern Indian Ocean are significantly becoming more evaporation dominant, particularly during the summer monsoon season, resulting in an increase of salt exported to the Southern Ocean.

1. Introduction

The two major basins that characterize the northern Indian Ocean (NIO) are the high-salinity Arabian Sea on the west and the significantly fresher Bay of Bengal on the east. The strong zonal sea surface salinity (SSS) gradient of the NIO is closely related to the regional dynamics of the hydrological cycle. Pisharoty (1965) and Ghosh et al. (1978) describe the moisture flux from the evaporation-dominant Arabian Sea to the Indian subcontinent by low-level monsoon winds (Tyagi et al., 2012). During the southwest (summer) monsoon season (June through September), this atmospheric circulation results in substantial precipitation over the Indian subcontinent and the Bay of Bengal. The Bay of Bengal receives major river runoff from the

Ganges, Brahmaputra, Godavari, Mahanadi, and Irravady (Varkey et al., 1996) and influences its SSS and the resultant high stratification in the mixed layer (Durand et al., 2007; Han et al., 2001; Kido & Tozuka, 2017; Pant et al., 2015; Sharma et al., 2007; Zhang et al., 2016).

The NIO is the only ocean that undergoes seasonal reversal of wind-driven circulation under the influence of seasonal reversal of monsoonal winds (Krishnamurti, 1979; Shankar et al., 2002). Seasonal current reversal is responsible for injection of high-salinity waters eastward from the Arabian Sea into the Bay of Bengal by the summer monsoon current (SMC) during southwest monsoon and flow of low salinity waters in the opposite direction by the winter monsoon current (WMC) during northeast monsoon (December–February), both of which are located at the southernmost point of India (Schott & McCreary, 2001; Shankar et al., 2002). Jensen (2001) determined maximal current speed of 0.6 m/s in the WMC in January and 1 m/s in the SMC in July and August when using a model to exclusively study the exchange of salt between the two basins and compared his model currents with an observational study by Schott et al. (1994). Murty et al. (1992) observed the influences of forcings such as low-level winds and river influx on property distributions in the Bay of Bengal and determined that the region north of 15°N and east of 89°E is strongly influenced by freshwater inputs from the surface up to 40- to 90-m depths and advection by wind-driven circulation south of 15°N.

Previous decadal studies of the Indian Ocean have historically focused on sea surface temperature (SST) and the Indian Ocean Dipole (IOD) due to the relationship between high SSTs and atmospheric deep convection. Clark et al. (2000) examined the relationship between decadal SST variability and its association to monsoon activity and found a positive correlation in the tropical Indian Ocean. Ashok et al. (2004) opined that decadal variability is of importance when observing IOD events. Kucharski et al. (2006) expounded on the results of both these studies by describing the mechanism between anomalous SST events on Hadley cell circulation and NIO rainfall.

There are two major studies regarding decadal change in salinity in the NIO. Boyer et al. (2005) analyzed salinity measurements from the World Ocean Database 2001 to determine linear trends in salinity for the World Ocean from 1955 to 1998 from the surface up to 3,000-m depth. They detected increased salinification at all latitudes in the upper 150 m and subsurface freshening south of the equator from 250- to 1,000-m depth. Durack and Wijffels (2010) noted a global trend of SSS increase in evaporation-dominated regions and SSS decrease in precipitation-dominated regions, indicating a strengthening of the global water cycle. They detected increasing salinity in the Arabian Sea and freshening in the Bay of Bengal. However, an analysis of the mechanisms of salt transport in the Indian Ocean by Nyadjro et al. (2011) determined a significant influence of zonal advection and freshwater forcings on SSS variability, which must be considered when studying the long-term dynamics of the upper layers of the NIO.

Our objective in this study is to conduct a decadal and large-scale analysis of salinity in the Indian Ocean and the corresponding physical mechanisms using Simple Ocean Data Assimilation (SODA) and HYbrid Coordinate Ocean Model (HYCOM). This research improves upon previous understanding of salinity trends on a decadal time scale by connecting the decadal trends of major regions of the NIO to the regional atmospheric and oceanic circulations. Here, we analyze decadal trends in the exchange of high- and low-salinity waters between the two NIO basins from 1993 to 2012 from a new perspective—that of four major water masses: the high-salinity Arabian Sea water (60–69°E, 12–22°N), basin exchange region (70–85°E, 4–10°N), the low-salinity Bay of Bengal water (84.5–94°E, 12–21°N), and the low-salinity Indonesian Throughflow (ITF; 91–101°E, 5–15°S). The rest of the paper is organized as follows. Section 2 and its subsections outline the data sets and methodology used in our research. We investigate the hydrological cycle in section 3. Section 4 explores salinity variability, and section 5 presents transports as a function of depth. Section 6 discusses our findings regarding depth-integrated transports. Section 7 concentrates on decadal salinity trends. Section 8 provides a summary and conclusion of this study.

2. Data and Methods

2.1. In Situ Observations

Global monthly streamflow data for the world's largest 925 rivers were used in this study from the National Centers for Atmospheric Research's Dai and Trenberth Global River Flow and Continental Discharge

Dataset. This data set includes observations from those described in Dai and Trenberth (2002), Dai et al. (2009), and the Global Runoff Data Centre. The Global Runoff Data Centre database consists of more than 9,000 stations and is the most comprehensive global streamflow data available (Dai, 2017). The Dai and Trenberth Global River Flow and Continental Discharge Dataset is lauded by Papa et al. (2012) as an accurate estimate of continent-to-ocean freshwater flux and is similar to other estimates of the Ganges-Brahmaputra discharge (Fekete et al., 2000; Vörösmarty et al., 1996). Chaitanya et al. (2014) also refer to both the Papa et al. (2012) and the Dai and Trenberth Global River Flow and Continental Discharge Dataset for accurate climatological discharges in this region. The Ganges-Brahmaputra river discharge in this data set was from 1956 to 1996, for which we used the full time period.

2.2. HYCOM Model and Reanalysis Data

Monthly outputs from a reanalysis version of HYCOM (https://hycom.org) fields with a horizontal resolution of 1/12° (about 7 km at the midlatitudes and ~8 km at the equator) and 41 layers in the vertical were used to compute salt and volume transports from January 1993 to December 2012. HYCOM was derived from the Miami Isopycnic Coordinate Ocean Model, as described in Bleck and Boudra (1981) and Bleck and Benjamin (1993). The full description of HYCOM can be found in Metzger et al. (2014). HYCOM uses a hybrid isopycnal/σ/z coordinate system that is isopycnal in the open stratified ocean, uses a terrain-following coordinate in shallow coastal regions, and z-level coordinates in the mixed layer. This coordinate system permits intersecting sloping topography by allowing zero-thickness layers in order to improve modeling of ocean dynamics due to more accurate simulation of local processes, particularly in coastal regions (Chassignet et al., 1996). The Navy Coupled Ocean Data Assimilation system is used to assimilate available satellite altimetry (courtesy of the Naval Oceanographic Office Altimeter Data Fusion Center), satellite and in situ SST, Expendable Bathythermograph in situ vertical temperature profiles, Argo floats, and moored buoys (Cummings, 2005). Atmospheric forcings are from the Navy Global Environmental Model (Hogan et al., 2014). The global version of HYCOM we are using is mesoscale-eddy resolving, and it allows for ITF, so it is well suited to help us address our questions of interest. As eddies have a broad range of scales from 1,000 km down to 1 cm, this data set cannot resolve microturbulent eddies but is appropriate for modeling mesoscale features (Torres et al., 2018).

For a decadal analysis, monthly SODA reanalysis version 3.3.1 temperature, salinity, and subsurface currents from 1993 to 2012 were used, and mapped onto a 0.25° × 0.25° Mercator horizontal grid at 50 vertical levels. This version uses the global ocean/sea ice component of the GFDL CM2.5 coupled model (Delworth et al., 2012) and uses 15.4 million hydrographic profiles from the World Ocean Database 2013 and bathythermograph data as described in Levitus et al. (2009) as well as in situ and remotely sensed SST (Casey et al., 2010; Ignatov et al., 2016; Woodruff et al., 2011). The data assimilation algorithm is described in Carton and Giese (2008). SODA is forced by multiple analyses, including NASA's Modern-Era Retrospective Analysis for Research And Applications Version 2 (Gelaro et al., 2017), the European Center for Medium Range Weather Forecast's atmospheric reanalysis interim product (ERA-Interim; Dee et al., 2011), DRAKKAR Forcing Set 5.2 (Dussin et al., 2016), the Coordinated Ocean Research Experiments Version 2 (Large & Yeager, 2004), and the Japan Meteorological Agency 55 year reanalysis (Kobayashi et al., 2015).

In HYCOM and SODA, the Palk Strait is open. Models used for transport calculations typically close the Palk Strait due to its negligible flow, so leaving it open provides an opportunity for HYCOM and SODA to overestimate its flow (Kurian & Vinayachandran, 2007; Rao et al., 2011). However, despite opening the Palk Strait, HYCOM and SODA are both commonly used for transport calculations in the Indian Ocean (Carton & Giese, 2008; D'Addezio et al., 2015; Grunseich et al., 2011; Nyadjro et al., 2011; Nyadjro et al., 2013; Trenary & Han, 2008). Additionally, the first layer of each model (1-m depth in HYCOM and 5-m depth in SODA) is adequate for resolving the SSS (Cahyarini et al., 2008; Grunseich et al., 2011; Melzer & Subrahmanyam, 2015; Nyadjro et al., 2013; Yuhong et al., 2013).

Evaporation and precipitation data sets used in this study are sourced from the European Centre for Medium-Range Weather Forecasting's ERA-Interim reanalysis monthly data set from 1993 to 2012 at a horizontal resolution of 1° × 1°. The ERA-Interim atmospheric reanalysis is coupled to an ocean-wave model and has improved outputs of the hydrological cycle than its predecessor ERA-40 (Berrisford et al., 2011).

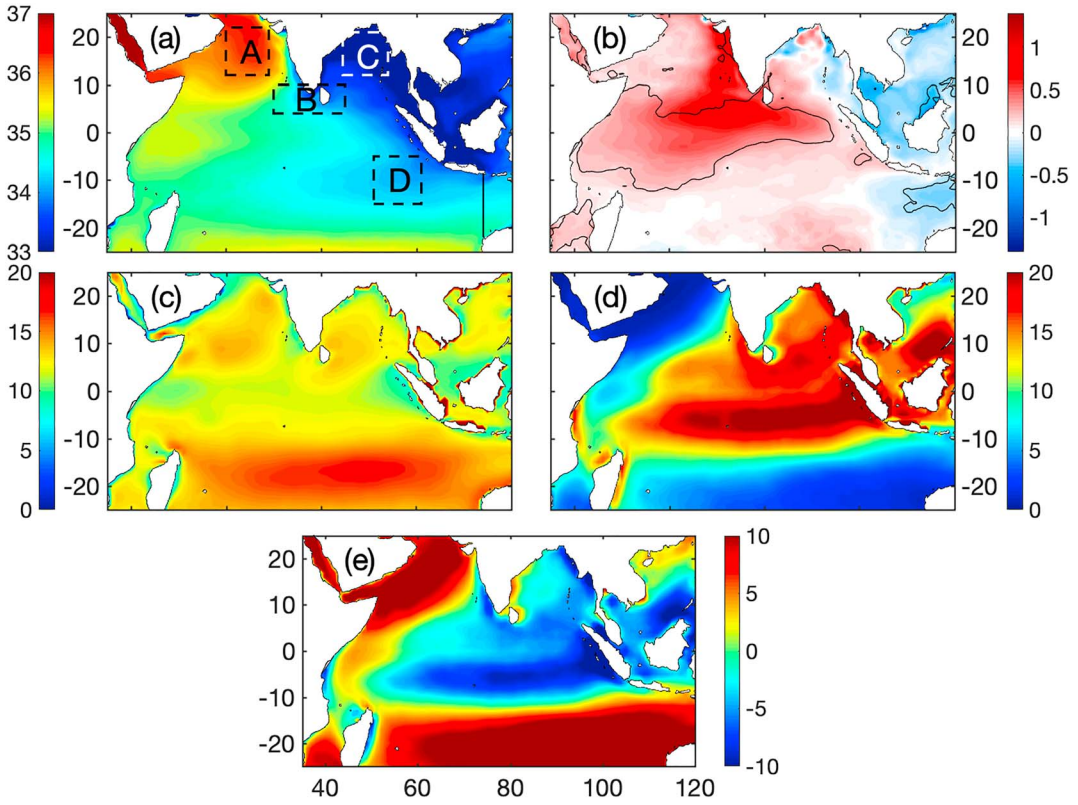

Figure 1. Mean annual (a) Simple Ocean Data Assimilation sea surface salinity, (b) coefficients of regression of Simple Ocean Data Assimilation sea surface salinity from 1993 to 2012 based on a linear trend (psu/decade), (c) evaporation (mm/day), (d) precipitation (mm/day), and (e) evaporation minus precipitation (mm/day). Boxes A–D denote the regions of study, and the black line at 114°E in panel (a) denotes the region where Indonesian Throughflow transports are computed. Black contours in panel (b) show regions where the linear trend is significant under an alpha of 0.05.

2.3. Methods

Zonal SSS transport was computed using the approach presented in Nyadjro et al. (2011). These authors evaluated transports using the surface salinity budget, directly evaluating transports from zonal hydrographic sections, and estimating the divergence of meridional transport. To compute the depth-integrated zonal salt transport (F_s) for SODA and HYCOM layers, each layer was integrated using

$$F_s = \int_{-H}^{z_0} \int_0^L \rho.u(y,z).S(y,z)dydz, \quad (1)$$

where ρ is the sea surface density (1,023 kg/m^3), S is salinity (defined as $\times 10^{-3}$ to ensure proper units of surface salinity transport), and u is zonal velocity (m/s) for each depth layer. H is the water depth (here taken as the ocean floor in depth-integrated transports), z_0 is the ocean surface, and L is the meridional expanse (m). Additional elaboration on this method can be found in Nyadjro et al. (2011).

Volume transport (F_v) in Sv (1 Sv = 10^6 m^3/s) was computed using

$$F_v = \int_{-H}^{z_0} \int_0^L u(y,z)dydz, \quad (2)$$

using the same defined variables as equation (1).

We applied an empirical orthogonal function (EOF) analysis to better understand the spatial and temporal variability of SSS in the Indian Ocean over the period of study from January 1993 to December 2012. EOF analysis is a statistical method that uses orthogonal eigenvectors to determine the percentage of variance

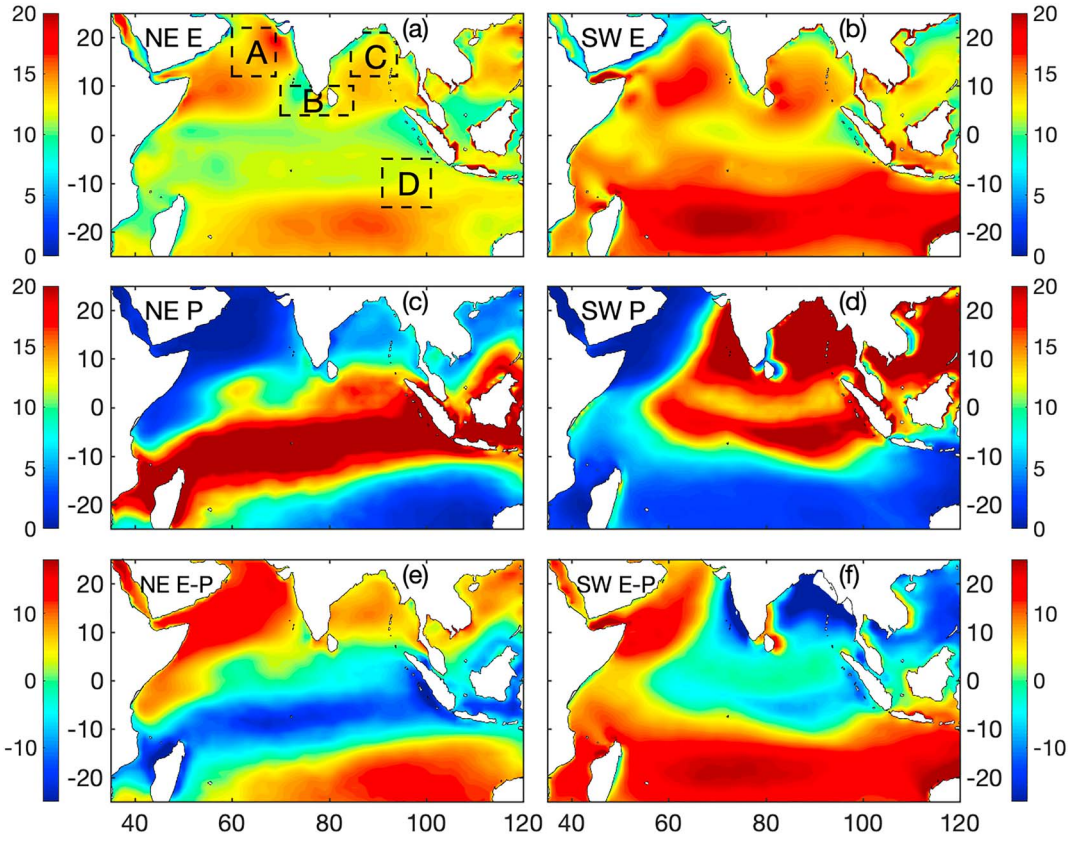

Figure 2. Mean seasonal climatologies of European Centre for Medium-Range Weather Forecasting evaporation (E; top row), precipitation (P; middle row), and evaporation minus precipitation (E-P; bottom row) for the NE (left) and SW (right) monsoon seasons (all in mm/day) over the period 1993–2012.

in the data set of the analyzed parameter into modes of variability, which can then be connected to physically relevant patterns rather than noise based on previous research. Our EOF of a single field is derived from the work of Bjornson and Venegas (1997). Decadal trends from January 1993 to December 2012 were estimated using a least squares linear regression fit (Dytham, 2011; Watson, 1967). To test trend significance at the 95% confidence level, an alpha of 0.05 was used.

3. Hydrological Cycle and SSS in the Indian Ocean

Figure 1a shows the mean annual variation of SODA SSS in the Indian Ocean highlighting the differences in the freshwater fluxes in the basins of NIO and low-salinity region in the southern tropical Indian Ocean. The Arabian Sea is characterized with high salinity, as it is an evaporation-dominant basin, and the Bay of Bengal is a precipitation (plus river runoff)-dominant low-salinity basin. The regions selected for this study to analyze changes in salinity are shown in Figure 1a. These regions are the high-salinity waters of the Arabian Sea (Box A), the seasonal salinity exchange between the Arabian Sea and Bay of Bengal (Box B), the fresher Bay of Bengal waters (Box C), and the ITF (Box D). The ITF is a westward current driven by the upper-level pressure gradient between the western equatorial Pacific and eastern equatorial Indian Ocean (Schott & McCreary, 2001). From the 1993 to 2012 linear trend in SSS distribution (Figure 1b), we find an overall positive linear salinity trend (determined by the mean slope value of the regression equation at each 1° × 1° grid), which is very high in the southeastern Arabian Sea and the central equatorial Indian Ocean (Figure 1b). The linear trend is significant at the 95% confidence level from the Somali Current region to the eastern equatorial Indian Ocean and southwestern Indian Ocean (Figure 1b).

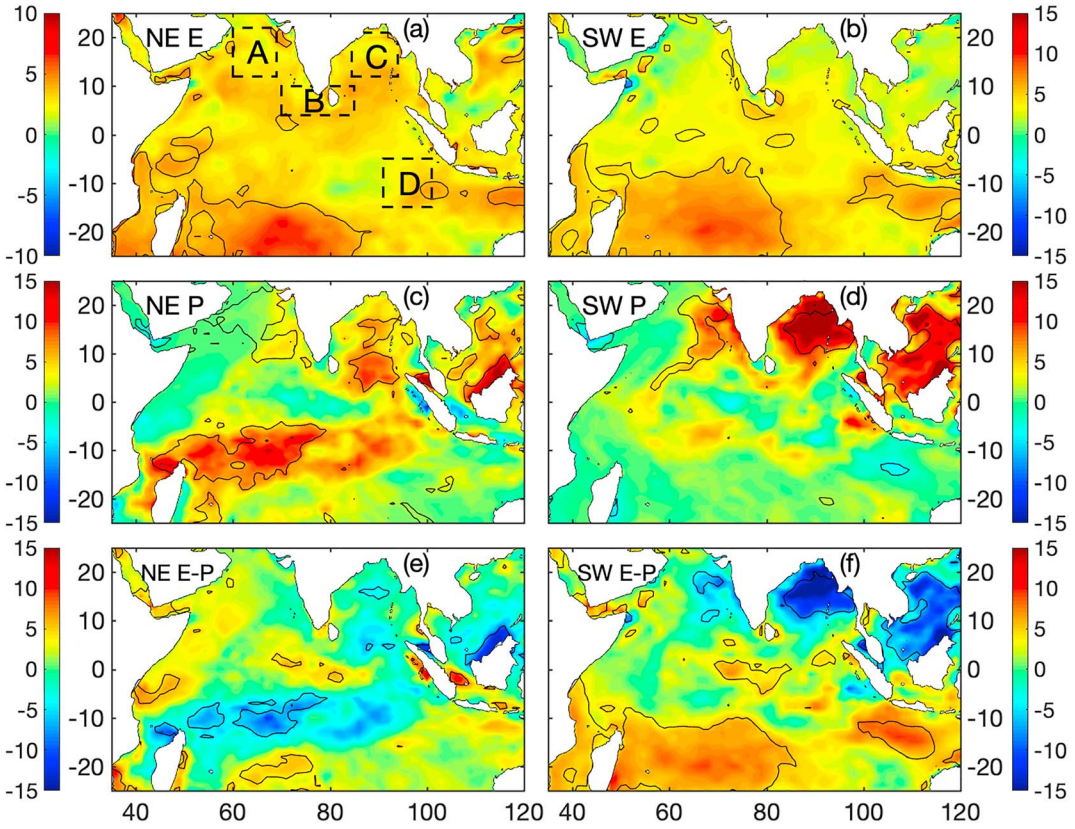

Figure 3. Coefficients of regression (denoting the slopes of each regression line at each grid cell) for the parameters in Figure 2 based on a linear trend (all in millimeters per day per decade). Black contours show regions where the linear trend is significant under an alpha of 0.05. E = evaporation; P = precipitation; E-P = evaporation minus precipitation.

Climatological evaporation (E; Figure 1c), precipitation (P; Figure 1d), and evaporation minus precipitation (E-P; Figure 1e) are presented to illustrate the spatial relationship between SSS and regional atmospheric processes. In the Arabian Sea, E-P is positive (Figure 1e) due to reduced precipitation (Figure 1d), while E-P in the Bay of Bengal (Figure 1e) is generally negative and responds more to the strong annual precipitation (Figure 1d). The exchange region between the two major basins also displays a negative E-P, though it is not as strong as the Bay of Bengal due to annual high precipitation (Figures 1d and 1e). Distribution of SSS in the ITF region is most similar to E and P when compared to the other three regions (Figure 1e). Its high precipitation is due to the presence of Intertropical Convergence Zone (Annamalai et al., 2003).

SSS in this region is highly responsive to the seasonal variations in evaporation (E; which leads to salinification) and precipitation (P; which leads to freshening). Figure 2 presents the climatologies of ECMWF E, P, and the E-P in the tropical Indian Ocean for the study period of 1993–2012. Evaporation is consistently high in the two basins during NE monsoon (December, January, and February) and SW monsoon (June, July, and August). In the NE monsoon, evaporation is the highest in the Arabian Sea, and in the SW monsoon it is high at 15°S and the southern Arabian Sea. Wintertime precipitation is constrained to the southern tropical Indian Ocean, but in the SW monsoon the precipitation is very heavy over Bay of Bengal, the northeastern quadrant of the Indian Ocean. The distributions of precipitation and evaporation in the NE monsoon cause the Box A (Arabian Sea) and Box C (Bay of Bengal) to be evaporation dominant from December through February. However, in the SW monsoon, the increased summertime heating causes stronger convection over NIO and leads to higher precipitation and the E-P distribution (Figure 2f), similar to that of its annual mean (Figure 1e).

To determine decadal changes in the seasonal hydrological cycle over the Indian Ocean, Figure 3 presents the 20-year linear decadal trend of E, P, and E-P with contoured regions where the trend is significant at a

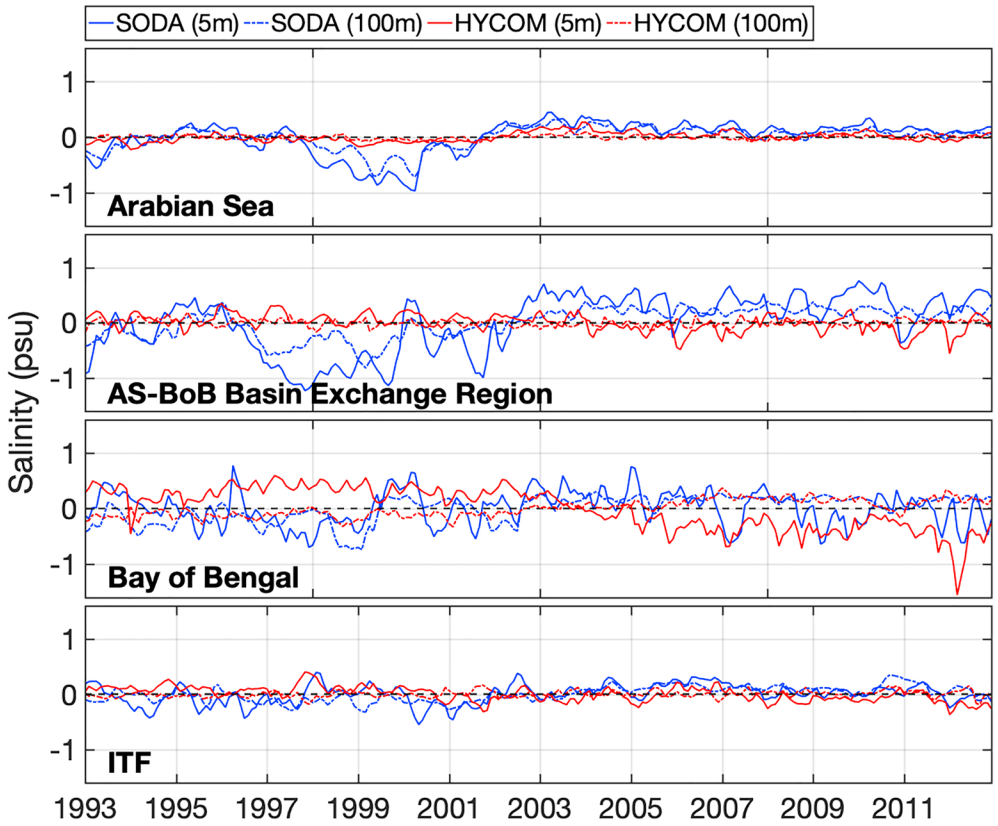

Figure 4. Box-averaged deseasonalized Simple Ocean Data Assimilation (SODA; in blue) and HYbrid Coordinate Ocean Model (HYCOM; in red) salinity anomalies from 1993 to 2012 for the Arabian Sea (60–69°E, 12–22°N), Arabian Sea and Bay of Bengal basin exchange region (70–85°E, 4–10°N), the Bay of Bengal (84.5–94°E, 12–21°N), and Indonesian Throughflow (ITF; 91–101°E, 5–15°S) at 5 m (solid lines) and 100 m (dashed lines). Salinity anomalies were computed with respect to decadal monthly mean values to remove the seasonal cycle.

95% confidence level. The trend (determined by the mean slope value of the linear regression equation at each grid point) in each parameter was calculated for each grid, and the increase in each parameter over the entire period is shown. Our most notable results indicate an increase in precipitation during both monsoon seasons, resulting in a more precipitation-dominated (and ultimately fresher) Indian Ocean in 2012 than 1993. Trends in evaporation are statistically significant at a 95% confidence level in the southern Indian Ocean (as is that of precipitation during the NE monsoon). The increasing precipitation trend in the northeastern Indian Ocean during the SW monsoon is statistically significant at the 95% confidence level. When comparing the E-P linear trends, the SW monsoon shows significantly stronger evaporation-dominated conditions east of Madagascar and significantly stronger precipitation-dominated conditions in the Bay of Bengal, all using a 95% confidence interval (Figure 3f).

4. Salinity Variability in the Tropical Indian Ocean

To better observe temporal variability in salinity in the four selected regions denoted in Figure 1, monthly box-averaged deseasonalized (using decadal means) SODA salinity anomalies from 1993 to 2012 at depths of 5 m and 100 m were computed (Figure 4). In the AS box, BoB box, and the AS-BoB exchange region, there is a variation between 1993 and 2003 with mostly negative SSS anomalies, and the large negative SSS peaks coincide with the IOD event of 1997–1998 (which is later discussed in an EOF analysis). Spatial shifts of convection in the equatorial Indian Ocean associated with IOD events directly impact salinity due to the new spatial distributions of evaporation and precipitation anomalies (anomalous winds also contribute greatly). The IOD events also impact salinity in the Indian Ocean indirectly via advection by the anomalously strong surface currents driven by the anomalous surface winds (Yu & Rienecker, 1999). During the

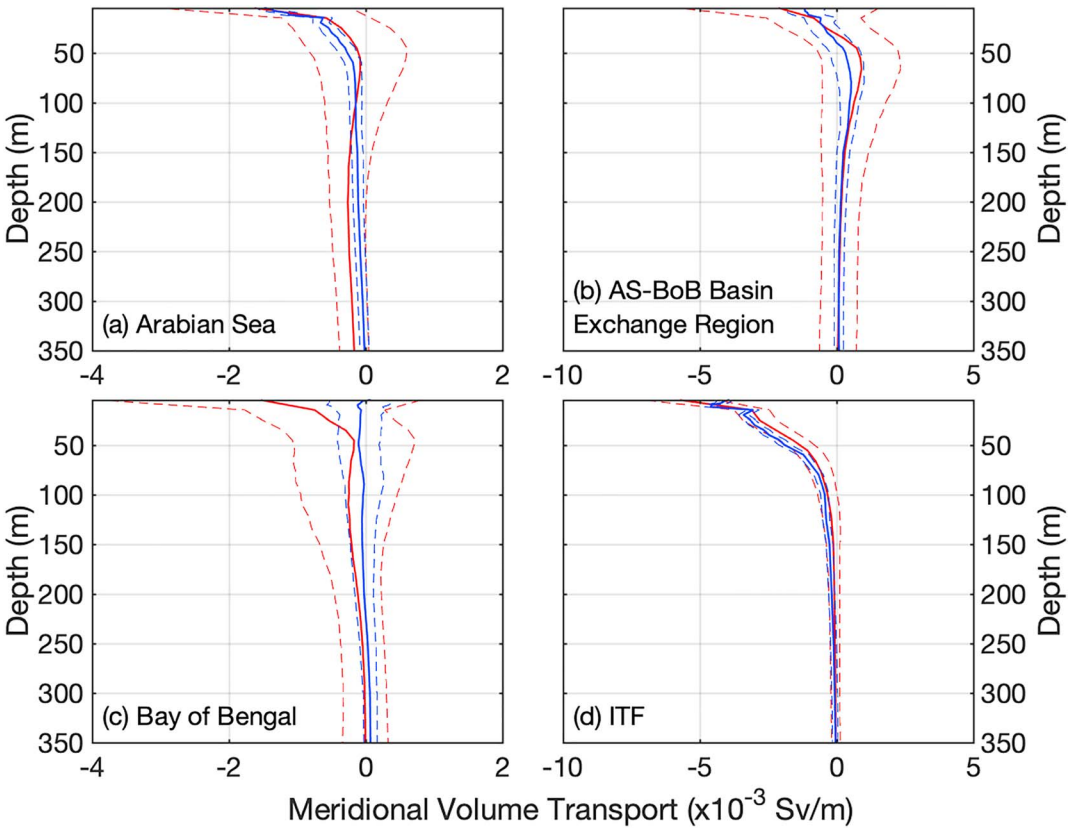

Figure 5. Box-averaged monthly meridional volume transport over the period of 1993 to 2012 standardized with depth for Simple Ocean Data Assimilation (red), and HYbrid Coordinate Ocean Model (blue) for (a) Box A, (b) Box B, (c) Box C, and (d) Box D (all marked in Figure 1a). *Y* axis is depth in meters, and dashed lines represent ±1 standard deviation. The standardization with unit depth is the reason for the units of Sverdrups per meter (Sv/m). Positive values signify northward transport and negative values signify southward transport. ITF = Indonesian Throughflow.

negative IOD events, westerly wind anomalies strengthen along the equator and help advection of Arabian Sea high-salinity waters toward Sumatra region (Yu & Rienecker, 1999). At the same time, low-salinity waters are injected into the Indian Ocean from the Western Pacific Ocean. This effect cascades across the entire Indian Ocean due to the presence of Rossby waves (Du & Zhang, 2015; Durand et al., 2013; Kido & Tozuka, 2017; Li et al., 2016). This is confirmed via Argo observations (Grunseich et al., 2011; Subrahmanyam et al., 2011) and model and reanalysis studies (Zhang et al., 2013). From the time series plots, one can see a change in SSS in the BoB in HYCOM and AS-BoB box in SODA (Figure 4). In the other two boxes, phase change is minimal at decadal scale (Figure 4). Hence, we can say that there is no appreciable decadal variation in SSS in the Arabian Sea and ITF region. Prior to deseasonalization, the 5- and 100-m salinities in both products show a significant seasonal cycle in variability as well as mean value, particularly in the basin exchange region, where standard deviations of SSS at 5-m depth were found to exceed 1 psu in both products, though the 100-m salinity standard deviation did not exceed 0.6 psu in the same region. Uncertainties were lowest in the ITF region (less than 0.4 psu standard deviation at both depth levels) and the Arabian Sea (boxed standard deviations less than 0.4 psu at 5-m depth and less than 0.25 psu at 100-m depth).

An important and interesting forcing that influences trends in SSS (and salinity throughout the mixed layer) is that of the vertical transport of salinity between the surface ocean and interior ocean, primarily driven by eddies. This applies to both mesoscale and submesoscale eddies, though mesoscale eddies tend to induce stronger vertical motions that act as a restoring force to restratify the mixed layer (Trott et al., 2019). However, the largest submesoscale vertical velocities associated with this phenomenon can penetrate 200 m below the mixed layer (Yu et al., 2019). Su et al. (2018) were able to globally resolve submesoscale heat transport on a global scale using a 1/48° resolution model and found that submesoscale dynamics are critically important for accurately estimating transports and better understanding Earth's climate.

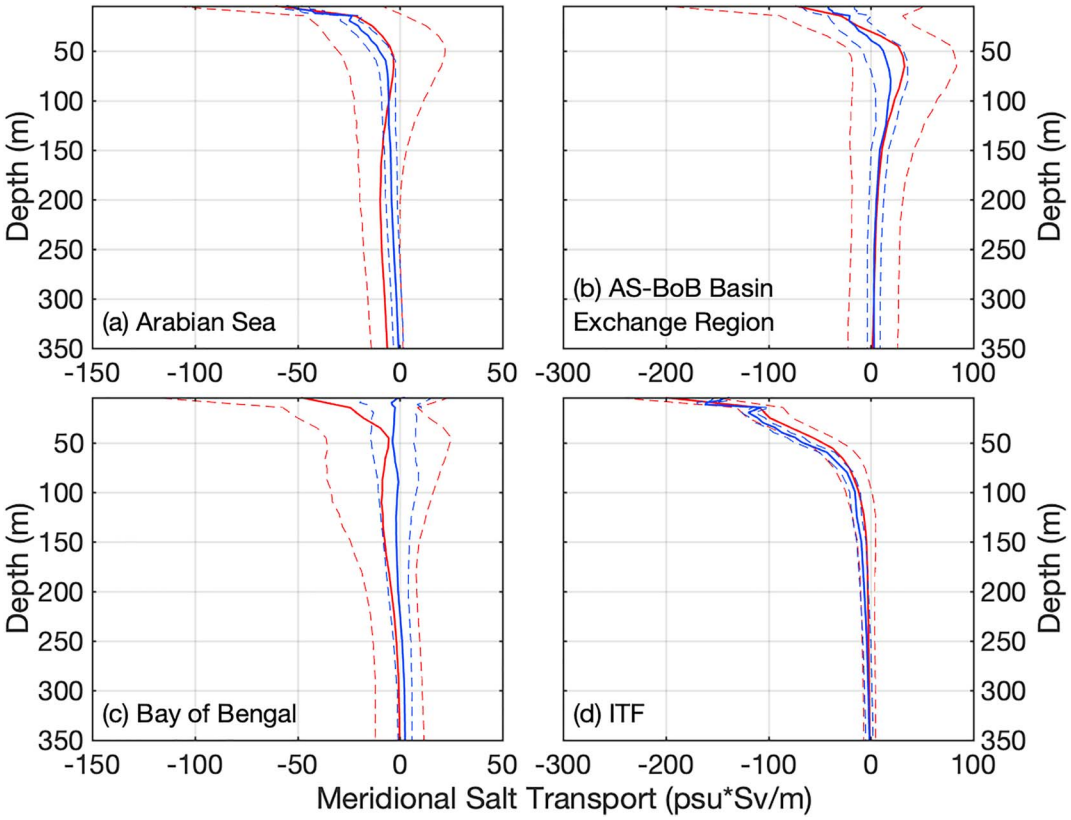

Figure 6. Same as Figure 5, but for salt transports (psu* Sverdrups per meter (Sv/m)).

5. Volume Transports

Meridional volume transport with depth down to 350 m in the four Box regions of study as computed using SODA and HYCOM is shown in Figures 5a–5d. All figures in this section are from January 1993 to December 2012 and are standardized with depth. This choice of depth limit was to show the strongest transports, as the meridional volume transports (standardized with depth) throughout the rest of the water column were relatively weak. This is expected in monsoonal regions, as the currents are primarily wind driven, hence the strongest transports at the surface (Figure 5). Results show a net southward flow near the surface in all boxes in SODA and HYCOM, but HYCOM shows a weak northward volume transport in the Arabian Sea at 40- to 110-m depth (Figure 5b) and relatively weak southward flow compared to SODA in the top 100 m of the BoB (Figures 6b). Both SODA and HYCOM show very similar distributions with depth of volume transport in the ITF region (Figure 5d). The ITF region had the most similar transport values between products and the narrowest margin of uncertainty, as both mean volume transports of the products were within 1 standard deviation of the other at all depth levels. Within all boxed regions, the HYCOM transports had smaller standard deviations and were consistently within one SODA standard deviation (Figure 5), which was also true of the meridional salt transports (Figure 6). The strongest meridional volume transports are in the basin exchange region within the top 300 m, likely from the East India Coastal Current and West India Coastal Current (as the WMC and SMC are primarily zonal currents) and in the top 100 m of the ITF region. However, box-averaged meridional volume transports are the strongest in the ITF region (Figure 5d). As Box D (Figure 1) is slightly north of the latitudes of strongest ITF westward transport (which is from 8.5°S to 22°S), it is likely that much of the southward transport of Box D is sourced from the Bay of Bengal (and not the ITF itself). Meridional salt transports with depth for the same box regions as in Figure 5 reveal identical depth profiles to that of volume transports (Figure 6).

The zonal depth-integrated salt and volume transports along the ITF region (114°E, 22°S to 8.5°S, identified in the 114°E section in Figure 1a) in SODA and HYCOM show different vertical distribution among the two

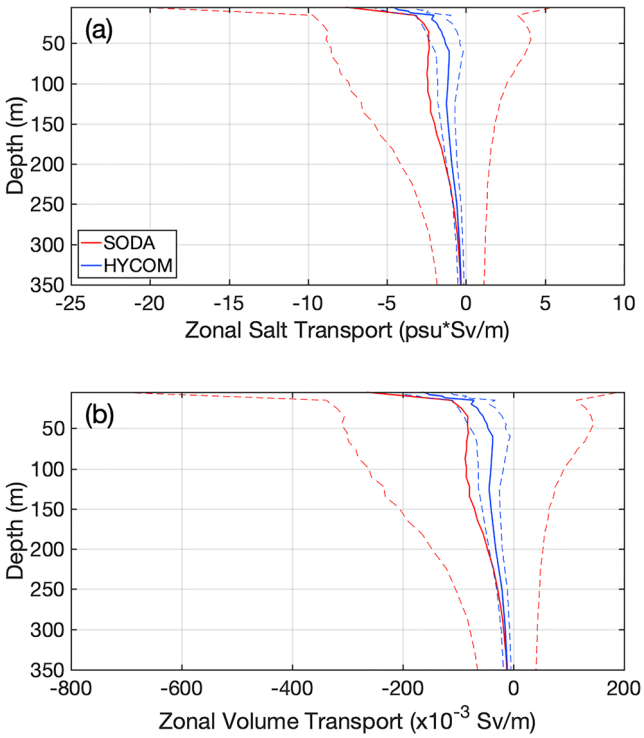

Figure 7. Zonal salt and volume transports normalized with depth for Simple Ocean Data Assimilation (SODA) and HYbrid Coordinate Ocean Model (HYCOM) along the Indonesian Throughflow region (114°E, 22°S to 8.5°S). Dashed lines represent ±1 standard deviation.

products, but consistently larger SODA estimates are seen for zonal salt and volume transports (Figure 7). Likely reasons for the differing results between the two products are to differing resolutions (both horizontally and vertically) and the difference in how the eddies are resolved. Eddying is a key component of overall buoyancy and salt fluxes (Klein et al., 2019); hence, the biggest difference in products (and largest range of uncertainty) is found within the top 100 m in all regions. It has been well observed that the effect of mesoscale eddying cascades to a variety of scales, ultimately influencing large-scale processes such as the ocean-scale decadal transports observed in this study (Klein et al., 2019). HYCOM's higher horizontal and vertical resolution likely contributes to a more accurate representation of the eddying transport component throughout the full Indian Ocean. Similarly, the HYCOM ITF transports were characterized by a smaller range of uncertainty (approximately one fourth that of SODA's). The ITF region is typically fresh due to high amounts of local precipitation (and from precipitation in the western Pacific Ocean).

6. Depth-Integrated Transports

The annual mean net meridional depth-integrated salt transports (Figure 8) in both SODA and HYCOM reveal that the tropical Indian Ocean is a net salt exporter to the equatorial region and southern tropical Indian Ocean. The northward (positive) and southward (negative) full depth-integrated SODA and HYCOM salinity transports (seen along the left and right of Figure 8) reveal salt convergence and divergence in the latitudinal bands (Figure 8). Due to its location of basin exchange, 8°N is the latitude at which transports enter and exit the two basins of the NIO. In the Arabian Sea, both products show a net salt transport out of the basin (Figure 8). This is not unexpected, as the source currents (the Somali Current in the summertime and the WMC feeding into the West India Coastal Current in the wintertime) are fresher than the Arabian Sea water mass (Figure 8). It is important to mention that to these transports one should note the Ekman transport, which is a function of surface winds. The annual mean Ekman transport is directed equatorward in the Indian Ocean across the 8°N section (Chereskin et al., 1997). The same effect is seen in the

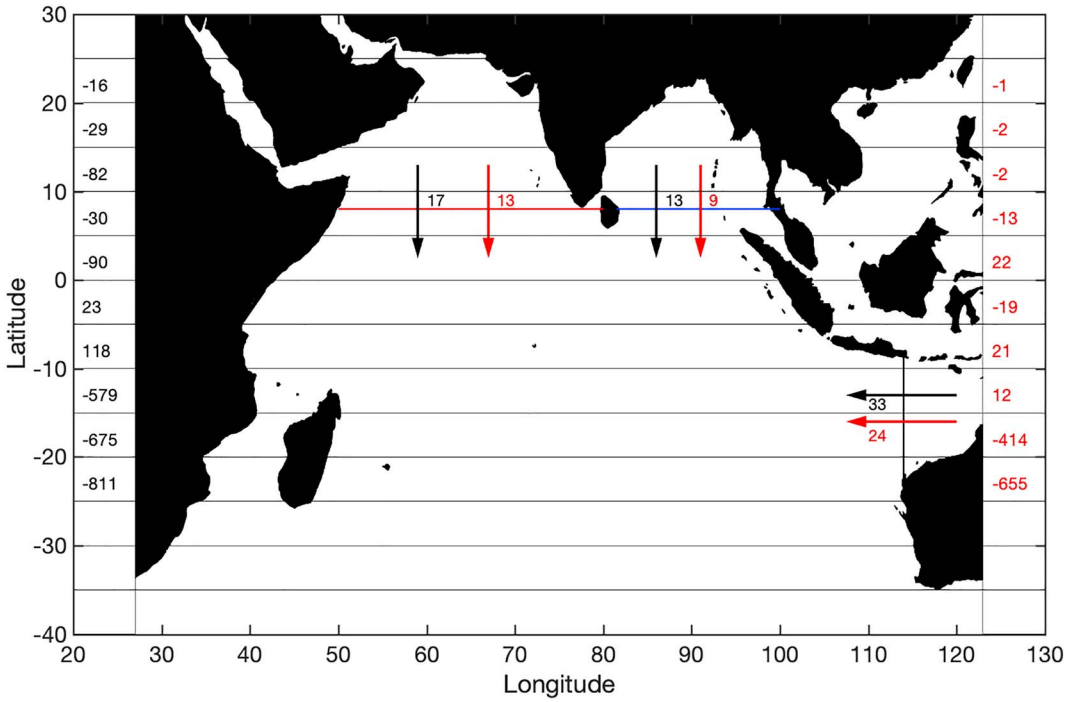

Figure 8. Annual mean depth-integrated net salt transports (psu Sv) from Simple Ocean Data Assimilation (black text and arrows) and HYbrid Coordinate Ocean Model (red text and arrows) across the 8°N latitude covering Arabian Sea basin (red line) and Bay of Bengal basin (blue line) and 114°E longitude in the Indonesian Throughflow region. Averages of meridional salt transports for each 5° latitudinal band (in psu Sv) on the left of the figure is for Simple Ocean Data Assimilation and along the right of the figure for HYbrid Coordinate Ocean Model.

BoB, where the depth-integrated transports for both products show increased salt also flowing out of the bay (Figure 8). As the currents in the ITF region are annually westward, it is not surprising that all transports are westward and into the Indian Ocean in both products (Figure 8). In both the products, the depth-integrated volume transports are same across 8°N section and in the ITF region. There is a discrepancy in the salt transports—one reason is the salinity changes in these products. The HYCOM salt transports are relatively weak. Salt convergence takes place between equator and 10°S in the SODA product (left-side scale in Figure 8) and between equator and 5°N in the HYCOM product (right-side scale in Figure 8).

Though the volume and salt transports showed nearly identical distributions with depth in all four boxed regions, there was notable latitudinal variation between the two transport types (Figures 9). Figure 9 compares SODA and HYCOM meridional salt and volume transports with latitude. In SODA meridional salt transport is southward south of 15°S, but in HYCOM there is a strong latitudinal variation, which impacted the latitudinally averaged bands in Figure 8 (Figure 9b). The same pattern is seen in the meridional volume transports of the two products (but at different magnitudes). The highest meridional transport variability was found at 10°N for both products due to the monsoonal current reversal, where the standard deviation of meridional salt transport was 10.0 psu Sv in SODA and 5.0 psu Sv in HYCOM. Depth-integrated meridional salt transports averaged over each 5° latitudinal band were outside of the margin of error for each product, though meridional salt transports at 6°N for each basin and zonal salt transports along the ITF region were within 1 standard deviation. This is likely due to the differing horizontal resolutions of the two products, which have similar results at individual latitudes and longitudes but show more stark differences when comparing spatial averages.

To determine the long-term trends of salt and volume transports in the Indian Ocean, linear trends of depth-integrated (from the surface to the ocean floor) zonal and meridional salt and volume transports were found during 1993–2012 using HYCOM (Figure 10) and SODA (Figure 11). The transport trends and regions of significance were very different between the two products. In HYCOM, the zonal salt and volume transports showed increasing westward flow about the equator and increasing eastward flow at approximately 5°S,

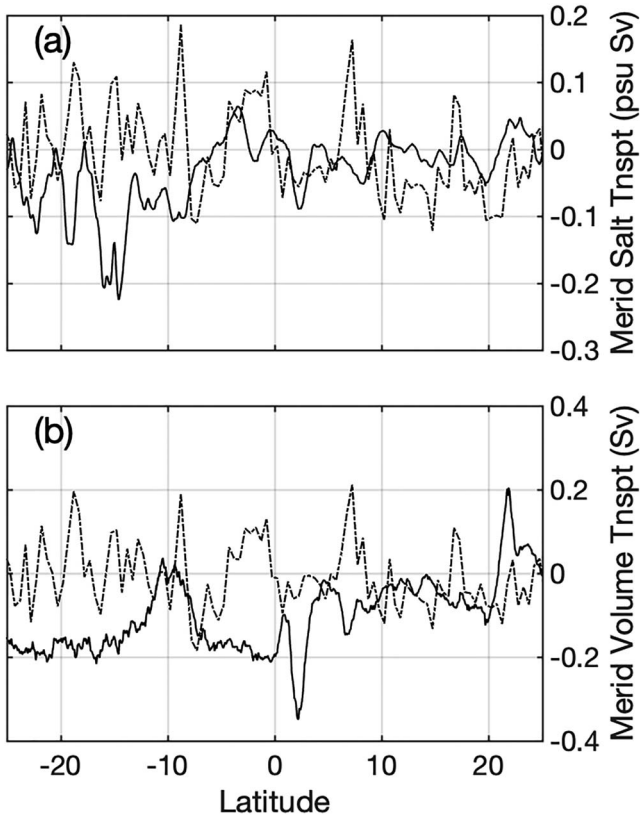

Figure 9. Comparison of latitudinal variation of transports between Simple Ocean Data Assimilation and HYbrid Coordinate Ocean Model in the Indian Ocean. Panel (a) is meridional salt transport, and panel (b) is meridional volume transport.

which could indicate northward shifting of the south Indian Gyre or (more likely, due to the full zonal extent across the Indian Ocean) latitudinal movement of the zonal equatorial currents. The standard error of the latitudinal variation of transports differed between the salt and volume transports. The standard error of the meridional salt transports was highest northward of the equator concurrent with high-salinity variability (0.03 and 0.02 psu Sv in SODA and HYCOM, respectively). The highest standard error for the volume transports was south of 10°S, a region of high eddy activity in the Indian Ocean associated with Agulhas retroflection (0.004 and 0.01 Sv in SODA and HYCOM, respectively). The highest-magnitude trends in the HYCOM meridional transports were in the southeastern Indian Ocean, which may be due to increased local eddying based on the spatial distribution of northward and southward transports. One possible reason for this is due to the fact that a key source of eddies is from the background potential energy. Wind-driven Ekman pumping and suction can change isopycnal slope and background potential energy, which can change eddy magnitude (Su et al., 2014; Su & Ingersoll, 2016). This process provides a valid mechanism for a decadal increase in eddy magnitude and the eddy component of transport in this region.

However, in SODA, the regions with the most significant trends were along the Somali Current and at the Somali Current outflow region in the central Arabian Sea (Figure 11). There is no significant trend in zonal equatorial currents in SODA zonal and meridional salt, and volume transports indicate an increased south-westerly Somali Current that advects waters sourced from the high salinity Arabian Sea water mass. In both HYCOM and SODA, the similar spatial relationship between the trends (including statistical significance at the 95% level) indicates that multidecadal trends in salinity transports are due to changes in local currents rather than changes in salinity. This is further supported via separation of the SSS and eddy kinetic energy trends throughout the Indian Ocean (Figure S1 in the supporting information). With the exception of the BoB, which is freshening due to increased precipitation, decadal salinification in the Indian Ocean is fairly

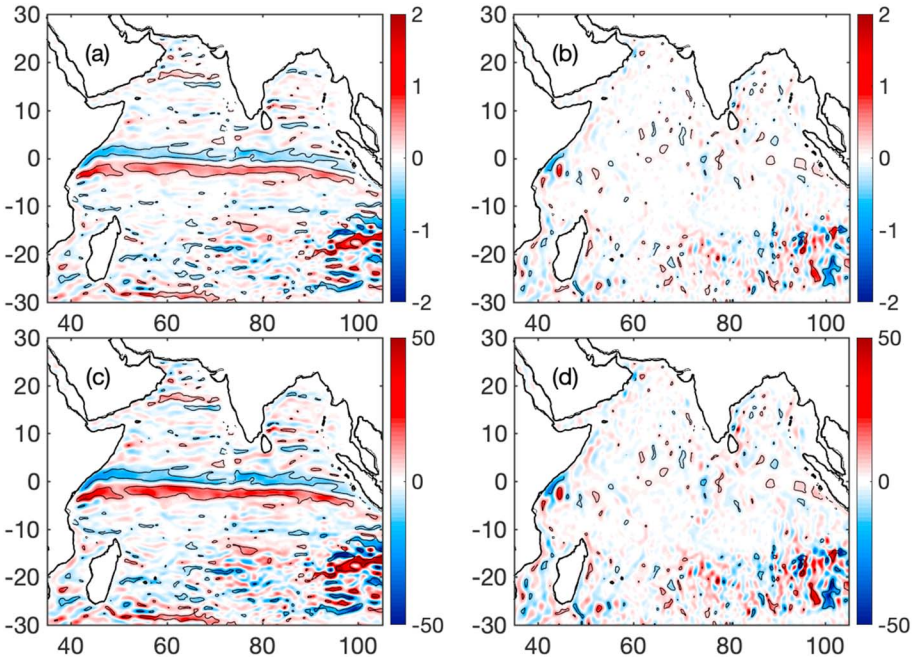

Figure 10. Coefficients of regression based on a linear trend for (a) zonal volume transports, (b) meridional volume transports, (c) zonal salt transports, and (d) meridional salt transports from 1993 to 2012 using HYbrid Coordinate Ocean Model. Black contours show regions where the linear trend is significant under an alpha of 0.05. Volume transport trends are in Sverdrups per decade (Sv/decade), and salt transport trends are in psu*Sverdrups per decade (Sv/decade). EOF = empirical orthogonal function.

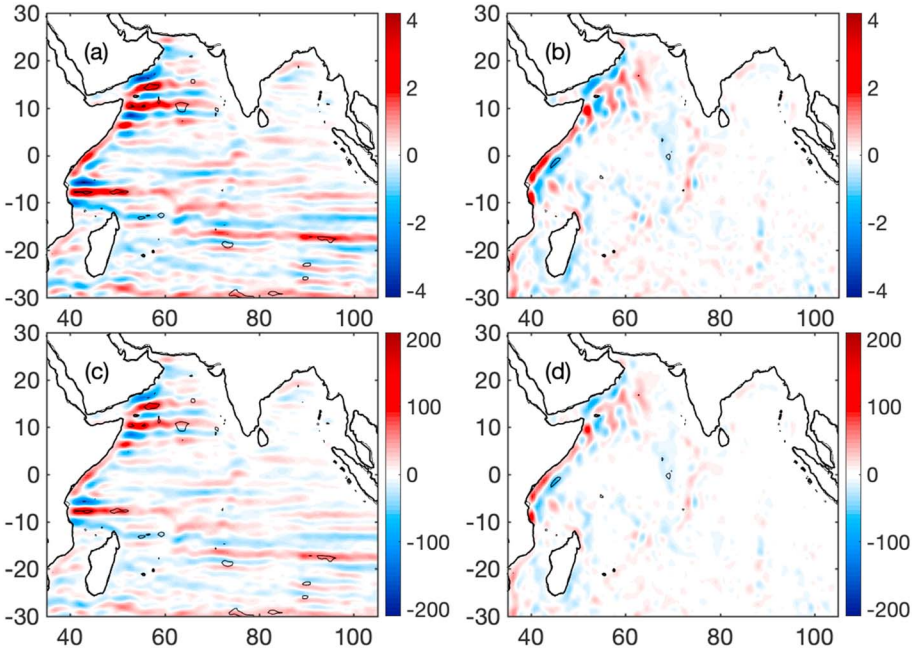

Figure 11. Coefficients of regression based on a linear trend for (a) zonal volume transports, (b) meridional volume transports, (c) zonal salt transports, and (d) meridional salt transports from 1993 to 2012 using Simple Ocean Data Assimilation. Black contours show regions where the linear trend is significant under an alpha of 0.05. Volume transport trends are in Sverdrups per decade (Sv/decade) and salt transport trends are in psu*Sverdrups per decade (Sv/decade).

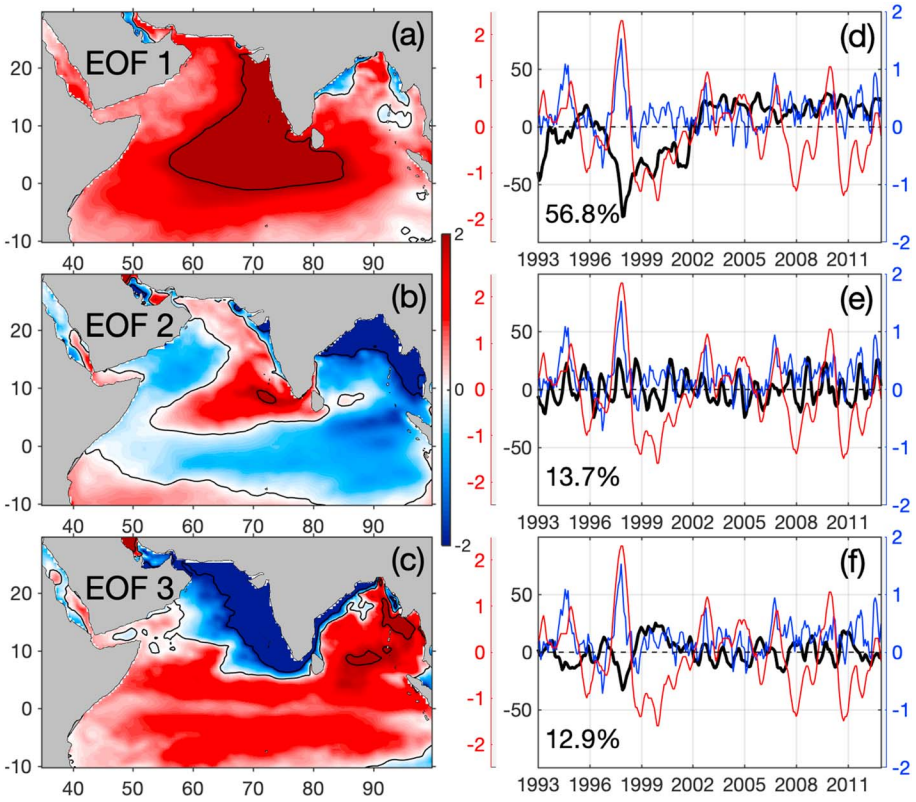

Figure 12. Empirical orthogonal function and principal components of monthly (1993–2012) Simple Ocean Data Assimilation sea surface salinity (a–c) and their temporal variability (d–f). Each map has been normalized (temporal eigenvectors set to one), and percentage of the total variance has been included. Blue time series is the Dipole Mode Index, and red time series is the El Niño 3.4 Index.

uniform, resulting in relatively unchanged salinity gradients. However, the trend in eddy kinetic energy over the same temporal period in both products reveals meridionally varying trends in the low latitudes of the Indian Ocean, indicating changes in equatorial currents that are statistically significant at the 95% level.

7. Decadal Trends in SSS

We have conducted EOF analysis on monthly SODA SSS of the NIO to better understand decadal variability in SSS (Figures 12a–12f). It appears that the NIO is undergoing an increase in salinity, in the most recent years with the most significant variability in the first mode to be concentrated in the region of the Arabian Sea Mini Warm Pool with the principal component (PC) analysis showing major freshening events in the 1990s. This is likely due to increased fresh water trapping from the Bay of Bengal in the southeastern region of the Arabian Sea, as there is increased fresh water in the BoB in recent years (though this trapping is only for 3 months—December–February; Subrahmanyam et al., 2011). This first EOF accounts for 56.8% of the total SSS variability for the region shown in Figure 12 and is due to ENSO and IOD events, as shown by the overlaid Dipole Mode Index (blue) and ENSO 3.4 Index (red). In the PC of the first EOF, there are large negative SSS events from 1993 to 2003 that signify freshening with peaks corresponding to IOD and ENSO events (Figure 12d). The exchange region (Figure 12a) shows large positive SSS despite the freshening events in the PC because the NIO experiences high salinity from 2003 to 2010, as seen in the PC for the first EOF. This region coincides likely with the large negative SSS in the PC (freshening events) during 1990–2003 that coincides with ENSO and IOD events. Similarly, the loading region in the Bay of Bengal also would correspond to salinification.

The second EOF accounts for 13.7% of the total variability. The second EOF shows a zonal dipole in the Arabian Sea with increasing salinity to the east and decreasing salinity to the west, consistent with a strengthening of surface currents during the summer monsoon (Figure 12b). During this time, relatively fresh equatorial waters feed into the Somali Current region (Trott et al., 2017) and the West India Coastal Current

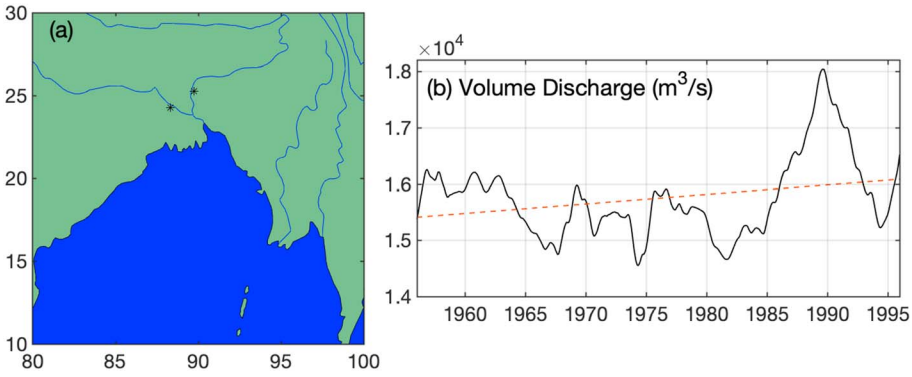

Figure 13. (a) The Ganges-Brahmaputra river system showing the two locations where river runoff was estimated and (b) sum of monthly volume discharge (m^3/s) at the stations denoted in panel (a).

advects the high-salinity northern Arabian Sea waters into the southeastern Arabian Sea region. Despite the application of a 10-year running mean to the monthly SODA SSS, this is a clearly seasonal cycle, as confirmed by the second PC (Figure 12e). The third EOF, which accounts for 12.9% of the variability, seems to imply separate salinification trends in the central and eastern Arabian Sea and the rest of the NIO (Figure 12c). The third PC also indicates that this is due to IOD events.

River discharge from major systems (particularly the Ganges-Brahmaputra) strongly influences the salinity of the basin on a decadal scale. Figure 13 shows the 41-year time series of annual river discharge from two stations from 1956 to 1996. The 41-year linear trend of this data indicates increasing discharge at a rate of 5,730 m^3/s per decade, which directly leads to decadal changes in salinity (Vinayachandran et al., 2015). This trend is significant at the 95% confidence level. Decreases in the major source of fresh water into the northern Bay of Bengal are sure to have significant impacts on the local salinity and regional mixed layer structure. There appears to be a decadal oscillatory signal in the Ganges-Brahmaputra river discharge with peaks approximately 15 years apart. The positive trend in Ganges-Brahamputra river runoff over the 41 years shows increases in freshwater flux, causing decrease in salinity. This contradiction may be explained due to the fact that the G-B river runoff during the recent decades might be reduced.

8. Conclusions

In this study, we conducted a decadal analysis of salinity in the Indian Ocean using SODA and HYCOM. To more accurately describe the spatial and temporal salinity changes, we examined four major bodies of water —the Arabian Sea (60–69°E, 12–22°N), the AS-BoB basin exchange region (70–85°E, 4–10°N), the Bay of Bengal (84.5–94°E, 12–21°N), and the ITF (91–101°E, 5–15°S). We compared E and P that change oceanic SSS with an emphasis on the hydrological cycle to determine how changes in spatial dominance of evaporation and precipitation relate to SSS distribution. We quantified the increasing magnitude of tropical precipitation and noted a statistically significant trend of increasing precipitation during the SW monsoon season over the Bay of Bengal, from 1993 to 2012.

Variability in salinity at 5- and 100-m depths in the four box regions of study were studied, finding that there was a higher-amplitude decadal signal in SODA at both depth levels than in HYCOM. SODA was also more responsive to IOD and ENSO events, which was later confirmed through an EOF analysis. Salt and volume transports for the four regions of study were compared with depth for SODA and HYCOM. We found the strongest transports in all regions of study to be zonal in the ITF region. Meridional salt transports with depth for the same box regions as in Figure 5 reveal identical depth profiles to that of volume transports. The depth-integrated zonal salt and volume transport for all products show similar vertical distributions.

Meridional full depth-integrated salt transports show that the southern tropical Indian Ocean is a net salt exporter over the period of 1993 to 2012. However, southward salt transport is not equal at all latitudes and varied in magnitude between the two products. There is some salinity compensation between the depth-integrated salt transports and the intensification of the hydrological cycle. While the changes in

evaporation and precipitation favor a stronger zonal salinity gradient in the NIO, the multidecadal salt and volume transports indicate an increase of freshwater into the saline Arabian Sea and increased salinity transports into the fresher BoB.

The biggest difference between the two products was seen when comparing the multidecadal transport trends between HYCOM and SODA. HYCOM noted the highest-magnitude significant trends to be in the zonal equatorial currents, while SODA noted more change in the Somali Current region. The spatial distribution of salt and volume transports for both products revealed that changes in salinity in this region (depth-integrated) are due to changes in local currents between the two products.

We applied EOF analysis to monthly SODA SSS in the NIO to determine spatial variability from 1993 to 2012. The first PC shows major freshening events in the 1990s and significant variability in the first mode in the Arabian Sea Mini Warm Pool region due to the influence of ENSO and IOD events. The second EOF is like that of monsoon currents, and the third mode is also due to IOD events, though with a different spatial pattern than the first EOF. There is a decadal signal of the Ganges-Brahmaputra river discharge over a 41-year period (1956–1996) with peaks approximately 15 years apart indicating increasing discharge at a rate of 5,730 m^3/s per decade.

Ultimately, the dominant forcing on SSS over a decadal time scale varies regionally throughout the Indian Ocean. Within the Arabian Sea and southern BoB, changes in E-P dominate changes in SSS. In the Arabian Sea where there is minimal riverine output, the salinification is purely due to an increase in evaporative rates that is not compensated by precipitation, but in the BoB the effect is twofold: first by direct local increases in precipitation, then by increased riverine outflow approximately 3 months following the peak of the summer monsoon season (Murty et al., 2004). In the exchange region between the Arabian Sea and BoB and along equatorial currents, there is significant current variability (both in magnitude and direction), so advection is the dominant term, with salinity transport trends responding more strongly to changes in local currents than changes in horizontal SSS gradients. In the southern Indian Ocean, large-scale changes in SSS are primarily due to an imbalance in E-P as the salinity transports are very weak due to the weak SSS gradients and weak mean currents, though there is a notable eddying transport component. Particularly in regions with high eddying (Somali Current, Agulhas retroflection), the salinity transport by eddies is a significant component of SSS variability. Advancements in model resolution and high-resolution satellite observations such as the Surface Water and Ocean Topography mission (to be launched in 2021) may someday more accurately resolve this transport component.

Acknowledgments
This work is supported by the ONR NASCar (Northern Arabian Sea Circulation-Autonomous Research) award N00014-15-1-2591 awarded to B. S. The author, V. S. N. Murty, is thankful to the director, CSIR-NIO, for his keen interest and support for this collaborative research work. SODA reanalysis product is from the University of Maryland (https://www.atmos.umd.edu/~ocean/index_files/soda3.3.1_mn_download.htm). HYCOM simulations are courtesy of NRL and J. S. ECMWF data sets were obtained from the ECMWF ERA-Interim data server (https://www.ecmwf.int/en/research/climate-reanalysis/reanalysis-climate-monitoring). J. S. was supported by the project "Earth System Prediction Capability" sponsored by the Office of Naval Research. Global monthly streamflow data used in this study are from the National Center for Atmospheric Research's (NCAR) Dai and Trenberth Global River Flow and Continental Discharge Dataset (https://rda.ucar.edu/datasets/ds551.0/). We are thankful for the helpful comments of the editor and two anonymous reviewers, which improved the quality of this paper.

References

Annamalai, H., Murtugudde, R., Potemra, J., Xie, S. P., Liu, P., & Wang, B. (2003). Coupled dynamics over the Indian Ocean: Spring initiation of the zonal mode. *Deep Sea Research Part II: Topical Studies in Oceanography*, *50*(12-13), 2305–2330. https://doi.org/10.1016/s0967-0645(03)00058-4

Ashok, K., Chan, W. L., Motoi, T., & Yamagata, T. (2004). Decadal variability of the Indian Ocean dipole. *Geophysical Research Letters*, *31*, L24207. https://doi.org/10.1029/2004gl021345

Berrisford, P., Dee, D., Poli, P., Brugge, R., Fielding, K., Fuentes, M., & Simmons, A. (2011). The ERA-Interim archive Version 20 ERA Report Series 1, Shinfield Park Reading, UK, 1317.

Bjornson, H., & Venegas, S. A. (1997). A manual for EOF and SVD—Analyses of climactic data.

Bleck, R., & Benjamin, S. G. (1993). Regional weather prediction with a model combining terrain-following and isentropic coordinates Part I: Model description. *Monthly Weather Review*, *121*(6), 1770–1785. https://doi.org/10.1175/1520-0493(1993)121%3C1770:rwpwam%3E2.0.co;2

Bleck, R., & Boudra, D. B. (1981). Initial testing of a numerical ocean circulation model using a hybrid (quasi-isopycnic) vertical coordinate. *Journal of Physical Oceanography*, *11*(6), 755–770. https://doi.org/10.1175/1520-0485(1981)011%3C0755:itoano%3E2.0.co;2

Boyer, T. P., Levitus, S., Antonov, J. I., Locarnini, R. A., & Garcia, H. E. (2005). Linear trends in salinity for the World Ocean 1955–1998. *Geophysical Research Letters*, *32*, L01604. https://doi.org/10.1029/2004gl021791

Cahyarini, S. Y., Pfeiffer, M., Timm, O., Dullo, W. C., & Schönberg, D. G. (2008). Reconstructing seawater δ18O from paired coral δ18O and Sr/Ca ratios: Methods, error analysis and problems, with examples from Tahiti (French Polynesia) and Timor (Indonesia). *Geochimica et Cosmochimica Acta*, *72*(12), 2841–2853. https://doi.org/10.1016/j.gca.2008.04.005

Carton, J. A., & Giese, B. S. (2008). A reanalysis of ocean climate using Simple Ocean Data Assimilation (SODA). *Monthly Weather Review*, *136*(8), 2999–3017. https://doi.org/10.1175/2007MWR1978.1

Casey, K. S., Brandon, T. B., Cornillon, P., & Evans, R. (2010). *The past, present, and future of the AVHRR Pathfinder SST program. Oceanography from Space: Revisited*, editors Barale V, Gower J.F.R, Albertoanza L, Springer, https://doi.org/10.1007/978-90-481-8681-5_16.0.

Chaitanya, A. V., Lengaigne, M., Vialard, J., Gopalakrishna, V. V., Durand, F., Kranthikumar, C., et al. (2014). Salinity measurements collected by fishermen reveal a "river in the sea" flowing along the eastern coast of India. *Bulletin of the American Meteorological Society*, *95*(12), 1897–1908. https://doi.org/10.1175/bams-d-12-00243.1

Chassignet, E. P., Smith, L. T., Bleck, R., & Bryan, F. O. (1996). A model comparison: Numerical simulations of the north and equatorial Atlantic oceanic circulation in depth and isopycnic coordinates. *Journal of Physical Oceanography*, *26*(9), 1849–1867. https://doi.org/10.1175/1520-0485(1996)026%3C1849:amcnso%3E2.0.co;2

Chereskin, T. K., Wilson, W. D., Bryden, H. L., Ffield, A., & Morrison, J. (1997). Observations of the Ekman balance at 8°30′N in the Arabian Sea during the 1995 southwest monsoon. *Geophysical Research Letters*, *24*(21), 2541–2544. https://doi.org/10.1029/97gl01057

Clark, C. O., Cole, J. E., & Webster, P. J. (2000). Indian Ocean SST and Indian summer rainfall: Predictive relationships and their decadal variability. *Journal of Climate*, *13*(14), 2503–2519. https://doi.org/10.1175/1520-0442(2000)013%3C2503:iosais%3E2.0.co;2

Cummings, J. A. (2005). Operational multivariate ocean data assimilation. *Quarterly Journal of the Royal Meteorological Society*, *131*(613), 3583–3604. https://doi.org/10.1256/qj.05.105

D'Addezio, J. M., Subrahmanyam, B., Nyadjro, E. S., & Murty, & V. S. N. (2015). Seasonal variability of salinity and salt transport in the northern Indian Ocean. *Journal of Physical Oceanography*, *45*(7), 1947–1966. https://doi.org/10.1175/jpo-d-14-0210.1

Dai, A. (2017). Dai and Trenberth Global River Flow and Continental Discharge Dataset. Research Data Archive at the National Center for Atmospheric Research, Computational and Information Systems Laboratory. https://doi.org/10.5065/D6V69H1T.

Dai, A., Qian, T., Trenberth, K. E., & Milliman, J. D. (2009). Changes in continental freshwater discharge from 1948 to 2004. *Journal of Climate*, *22*(10), 2773–2792. https://doi.org/10.1175/2008jcli2592.1

Dai, A., & Trenberth, K. E. (2002). Estimates of freshwater discharge from continents: Latitudinal and seasonal variations. *Journal of Hydrometeorology*, *3*(6), 660–687. https://doi.org/10.1175/1525-7541(2002)003%3C0660:eofdfc%3E2.0.co;2

Dee, D. P., Uppala, S. M., Simmons, A. J., Berrisford, P., Poli, P., Kobayashi, S., et al. (2011). The ERA-Interim reanalysis: Configuration and performance of the data assimilation system. *Quarterly Journal of the Royal Meteorological Society*, *137*(656), 553–597. https://doi.org/10.1002/qj.828

Delworth, T. L., Rosati, A., Anderson, W., Adcroft, A. J., Balaji, V., Benson, R., et al. (2012). Simulated climate and climate change in the GFDL CM2. 5 high-resolution coupled climate model. *Journal of Climate*, *25*(8), 2755–2781. https://doi.org/10.1175/jcli-d-11-00316.1

Du, Y., & Zhang, Y. (2015). Satellite and Argo observed surface salinity variations in the tropical Indian Ocean and their association with the Indian Ocean dipole mode. *Journal of Climate*, *28*(2), 695–713. https://doi.org/10.1175/jcli-d-14-00435.1

Durack, P. J., & Wijffels, S. E. (2010). Fifty-year trends in global ocean salinities and their relationship to broad-scale warming. *Journal of Climate*, *23*(16), 4342–4362. https://doi.org/10.1175/2010jcli3377.1

Durand, F., Alory, G., Dussin, R., & Reul, N. (2013). SMOS reveals the signature of Indian Ocean dipole events. *Ocean Dynamics*, *63*(11-12), 1203–1212. https://doi.org/10.1007/s10236-013-0660-y

Durand, M., Andreadis, K. M., Alsdorf, D. E., Lettenmaier, D. P., Moller, D., & Wilson, M. (2007). Estimation of bathymetric depth and slope from data assimilation of swath altimetry into a hydrodynamic model. *Geophysical Research Letters*, *35*, L20401. https://doi.org/10.1029/2008gl034150

Dussin, R., Barnier, B., Brodeau, L., & Molines, J. M. (2016). The making of the Drakkar Forcing Set DFS5. *DRAKKAR/MyOcean Report*, *16*, 01–04.

Dytham, C. (2011). *Choosing and using statistics: A biologist's guide*. John Wiley & Sons.

Fekete, B. M., Vörösmarty, C. J., & Grabs, W. (2000). Global, composite runoff fields based on observed river discharge and simulated water balances. Federal Institute of Hydrology.

Gelaro, R., McCarty, W., Suárez, M. J., Todling, R., Molod, A., Takacs, L., & Wargan, K. (2017). The modern-era retrospective analysis for research and applications version 2 (MERRA-2). *Journal of Climate*, *30*(14), 5419–5454. https://doi.org/10.1175/jcli-d-16-0758.1

Ghosh, S. K., Pant, M. C., & Dewan, B. N. (1978). Influence of the Arabian Sea on the Indian summer monsoon. *Tellus*, *30*(2), 117–125. https://doi.org/10.3402/tellusa.v30i2.10324

Grunseich, G., Subrahmanyam, B., Murty, V. S. N., & Giese, B. S. (2011). Sea surface salinity variability during the Indian Ocean Dipole and ENSO events in the tropical Indian Ocean. *Journal of Geophysical Research*, *116*, C11013. https://doi.org/10.1029/2011JC007456

Han, W., McCreary, J. P., & Kohler, K. E. (2001). Influence of precipitation minus evaporation and Bay of Bengal rivers on dynamics thermodynamics and mixed layer physics in the upper Indian Ocean. *Journal of Geophysical Research*, *106*(C4), 6895–6916. https://doi.org/10.1029/2000jc000403

Hogan, T. F., Liu, M., Ridout, J. A., Peng, M. S., Whitcomb, T. R., Ruston, B. C., et al. (2014). The Navy Global Environmental Model. *Oceanography*, *27*(3), 116–125. https://doi.org/10.5670/oceanog.2014.73

Ignatov, A., Zhou, X., Petrenko, B., Liang, X., Kihai, Y., Dash, P., Stroup, J., Sapper, J., & DiGiacomo, P. (2016). AVHRR GAC SST Reanalysis Version 1 (RAN1). *Remote Sensing*, *8*(4), 315. https://doi.org/10.3390/rs8040315

Jensen, T. G. (2001). Arabian Sea and Bay of Bengal exchange of salt and tracers in an ocean model. *Geophysical Research Letters*, *28*(20), 3967–3970. https://doi.org/10.1029/2001gl013422

Kido, S., & Tozuka, T. (2017). Salinity variability associated with the positive Indian Ocean Dipole and its impact on the upper ocean temperature. *Journal of Climate*, *30*(19), 7885–7907. https://doi.org/10.1175/jcli-d-17-0133.1

Klein, P., Lapeyre, G., Siegelman, L., Qiu, B., Fu, L. L., Torres, H., et al. (2019). Ocean-scale interactions from space. *Earth and Space Science*, *6*(5), 795–817. https://doi.org/10.1029/2018ea000492

Kobayashi, S., Ota, Y., Harada, Y., Ebita, A., Moriya, M., Onoda, H., et al. (2015). The JRA-55 reanalysis: General specifications and basic characteristics. *Journal of the Meteorological Society of Japan Series II*, *93*(1), 5–48. https://doi.org/10.2151/jmsj.2015-001

Krishnamurti, T. N. (1979). *Tropical meteorology*. Secretariat of the World Meteorological Organization. New York: Springer.

Kucharski, F., Molteni, F., & Yoo, J. H. (2006). SST forcing of decadal Indian monsoon rainfall variability. *Geophysical Research Letters*, *33*, L03709. https://doi.org/10.1029/2005gl025371

Kurian, J., & Vinayachandran, P. N. (2007). Mechanisms of formation of the Arabian Sea Mini Warm Pool in a high-resolution Ocean General Circulation Model. *Journal of Geophysical Research*, *112*, C05009. https://doi.org/10.1029/2006jc003631

Large, W. G., & Yeager, S. G. (2004). Diurnal to decadal global forcing for ocean and sea-ice models: the data sets and flux climatologies. Boulder: National Center for Atmospheric Research.

Levitus, S., Antonov, J. I., Boyer, T. P., Locarnini, R. A., Garcia, H. E., & Mishonov, A. V. (2009). Global ocean heat content 1955–2008 in light of recently revealed instrumentation problems. *Geophysical Research Letters*, *36*, L07608. https://doi.org/10.1029/2008GL037155

Li, J., Liang, C., Tang, Y., Dong, C., Chen, D., Liu, X., & Jin, W. (2016). A new dipole index of the salinity anomalies of the tropical Indian Ocean. *Scientific Reports*, *6*(1), 24260. https://doi.org/10.1038/srep24260

Metzger, E. J., Smedstad, O. M., Thoppil, P. G., Hurlburt, H. E., Cummings, J. A., Wallcraft, A. J., et al. (2014). US Navy operational global ocean and Arctic ice prediction systems. *Oceanography*, *27*(3), 32–43. https://doi.org/10.5670/oceanog.2014.66

Melzer, B. A., & Subrahmanyam, B. (2015). Investigating decadal changes in sea surface salinity in oceanic subtropical gyres. *Geophysical Research Letters*, *42*, 7631–7638. https://doi.org/10.1002/2015gl065636

Murty, V. S. N., Sarma, Y. V. B., Rao, D. P., & Murty, C. S. (1992). Water characteristics mixing and circulation in the Bay of Bengal during southwest monsoon. *Journal of Marine Research*, *50*(2), 207–228. https://doi.org/10.1357/002224092784797700

Murty, V. S. N., Subrahmanyam, B., Tilvi, V., & O'Brien, J. J. (2004). A new technique for the estimation of sea surface salinity in the tropical Indian Ocean from OLR. *Journal of Geophysical Research*, *109*, C12006. https://doi.org/10.1029/2003JC001928

Nyadjro, E. S., Subrahmanyam, B., & Giese, B. S. (2013). Variability of salt flux in the Indian Ocean during 1960–2008. *Remote Sensing of Environment*, *134*, 175–193. https://doi.org/10.1016/j.rse.2013.03.005

Nyadjro, E. S., Subrahmanyam, B., & Shriver, J. F. (2011). Seasonal variability of salt transport during the Indian Ocean monsoons. *Journal of Geophysical Research*, *116*, C08036. https://doi.org/10.1029/2011jc006993

Pant, V., Girishkumar, M. S., Bhaskar, T. U., Ravichandran, M., Papa, F., & Thangaprakash, V. P. (2015). Observed interannual variability of near-surface salinity in the Bay of Bengal. *Journal of Geophysical Research: Oceans*, *120*, 3315–3329. https://doi.org/10.1002/2014JC010340

Papa, F., Bala, S. K., Pandey, R. K., Durand, F., Gopalakrishna, V. V., Rahman, A., & Rossow, W. B. (2012). Ganga-Brahmaputra river discharge from Jason-2 radar altimetry: An update to the long-term satellite-derived estimates of continental freshwater forcing flux into the Bay of Bengal. *Journal of Geophysical Research*, *117*, C11021. https://doi.org/10.1029/2012JC008158

Pisharoty, P. R. (1965). Evaporation from the Arabian Sea and the Indian southwest monsoon. Proceedings of International Indian Ocean Expedition, 43-54.

Rao, R. R., Girishkumar, M. S., Ravichandran, M., Gopalakrishna, V. V., & Thadathil, P. (2011). Do cold, low salinity waters pass through the Indo-Sri Lanka Channel during winter? *International Journal of Remote Sensing*, *32*(22), 7383–7398. https://doi.org/10.1080/01431161.2010.523728

Schott, F., Reppin, J., Fishrer, J., & Quadfasel, D. (1994). Currents and transports of the Monsoon currents and transports of the Monsoon Current south of Sri Lanka. *Journal of Geophysical Research*, *99*(C12), 25,127–25,141. https://doi.org/10.1029/94JC02216

Schott, F. A., & McCreary, J. P. Jr. (2001). The monsoon circulation of the Indian Ocean. *Progress in Oceanography*, *51*(1), 1–123. https://doi.org/10.1016/s0079-6611(01)00083-0

Shankar, D., Vinayachandran, P. N., & Unnikrishnan, A. S. (2002). The monsoon currents in the north Indian Ocean. *Progress in Oceanography*, *52*(1), 63–120. https://doi.org/10.1016/s0079-6611(02)00024-1

Sharma, R., Agarwal, N., Basu, S., & Agarwal, V. K. (2007). Impact of satellite-derived forcings on numerical ocean model simulations and study of sea surface salinity variations in the Indian Ocean. *Journal of Climate*, *20*(5), 871–890. https://doi.org/10.1175/jcli4032.1

Su, Z., & Ingersoll, A. P. (2016). On the minimum potential energy state and the eddy size–constrained APE density. *Journal of Physical Oceanography*, *46*(9), 2663–2674. https://doi.org/10.1175/jpo-d-16-0074.1

Su, Z., Stewart, A. L., & Thompson, A. F. (2014). An idealized model of Weddell Gyre export variability. *Journal of Physical Oceanography*, *44*(6), 1671–1688. https://doi.org/10.1175/jpo-d-13-0263.1

Su, Z., Wang, J., Klein, P., Thompson, A. F., & Menemenlis, D. (2018). Ocean submesoscales as a key component of the global heat budget. *Nature communications*, *9*(1), 775. https://doi.org/10.1038/s41467-018-02983-w

Subrahmanyam, B., Murty, V. S. N., & Heffner, D. M. (2011). Sea surface salinity variability in the tropical Indian Ocean. *Remote Sensing of Environment*, *115*(3), 944–956. https://doi.org/10.1016/j.rse.2010.12.004

Torres, H. S., Klein, P., Menemenlis, D., Qiu, B., Su, Z., Wang, J., et al. (2018). Partitioning ocean motions into balanced motions and internal gravity waves: A modeling study in anticipation of future space missions. *Journal of Geophysical Research: Oceans*, *123*(11), 8084–8105. https://doi.org/10.1029/2018jc014438

Trenary, L. L., & Han, W. (2008). Causes of decadal subsurface cooling in the tropical Indian Ocean during 1961–2000. *Geophysical Research Letters*, *35*, L17602. https://doi.org/10.1029/2008gl034687

Trott, C. B., Subrahmanyam, B., & Murty, V. S. N. (2017). Variability of the Somali Current and eddies during the southwest monsoon regimes. *Dynamics of Atmospheres and Oceans*, *79*, 43–55. https://doi.org/10.1016/j.dynatmoce.2017.07.002

Trott, C. B., Subrahmanyam, B., & Nyadjro, E. S. (2019). Influence of mesoscale features on mixed layer dynamics in the Arabian Sea. *Journal of Geophysical Research: Oceans*, *124*, 3361–3377. https://doi.org/10.1029/2019JC014965

Tyagi, A., Asnani, P. G., De, U. S., Hatwar, H. R., & Mazumdar, A. B. (2012). The Monsoon Monograph (Volume 1 and 2). India Meteorological Department Report.

Varkey, M. J., Murty, V. S. N., & Suryanarayana, A. (1996). Physical oceanography of the Bay of Bengal and Andaman Sea. *Oceanographic Literature Review*, *5*(44), 413.

Vinayachandran, P. N., Jahfer, S., & Nanjundiah, R. S. (2015). Impact of river runoff into the ocean on Indian summer monsoon. *Environmental Research Letters*, *10*(5), 054008. https://doi.org/10.1088/1748-9326/10/5/054008

Vörösmarty, C. J., Fekete, B. M., Meybeck, M., & Lammers, R. B. (1996). Global system of rivers: Its role in organizing continental land mass and defining land-to-ocean linkages. *Global Biogeochemical Cycles*, *14*(2), 599–621. https://doi.org/10.1029/1999gb900092

Watson, G. S. (1967). Linear least squares regression. *The Annals of Mathematical Statistics*, *38*(6), 1679–1699. https://doi.org/10.1214/aoms/1177698603

Woodruff, S. D., Worley, S. J., Lubker, S. J., Ji, Z., Eric Freeman, J., Berry, D. I., et al. (2011). ICOADS Release 2.5: extensions and enhancements to the surface marine meteorological archive. *International Journal of Climatology*, *31*(7), 951–967. https://doi.org/10.1002/joc.2103

Yu, L., & Rienecker, M. M. (1999). Mechanisms for the Indian Ocean warming during the 1997-98 El Nino. *Geophysical Research Letters*, *26*(6), 735–738. https://doi.org/10.1029/1999gl900072

Yu, X., Naveira Garabato, A. C., Martin, A. P., Buckingham, C. E., Brannigan, L., & Su, Z. (2019). An annual cycle of submesoscale vertical flow and restratification in the upper ocean. *Journal of Physical Oceanography*, *49*(6), 1439–1461. https://doi.org/10.1175/jpo-d-18-0253.1

Yuhong, Z., Yan, D., Shaojun, Z., Yali, Y., & Xuhua, C. (2013). Impact of Indian Ocean Dipole on the salinity budget in the equatorial Indian Ocean. *Journal of Geophysical Research: Oceans*, *118*, 4911–4923. https://doi.org/10.1002/jgrc.20392

Zhang, Y., Du, Y., & Qu, T. (2016). A sea surface salinity dipole mode in the tropical Indian Ocean. *Climate Dynamics*, *47*(7-8), 2573–2585. https://doi.org/10.1007/s00382-016-2984-z

Zhang, Y., Du, Y., Zheng, S., Yang, Y., & Cheng, X. (2013). Impact of Indian Ocean dipole on the salinity budget in the equatorial Indian Ocean. *Journal of Geophysical Research: Oceans*, *118*, 4911–4923. https://doi.org/10.1002/jgrc.20392